



Soft Matter

The Influence of Curvature on Domain Distribution in Binary Mixture Membranes

Journal:	<i>Soft Matter</i>
Manuscript ID	SM-ART-06-2019-001262
Article Type:	Paper
Date Submitted by the Author:	24-Jun-2019
Complete List of Authors:	Li, Wei; Oak Ridge National Laboratory, Center for Nanophase Materials Sciences Carrillo, Jan Michael; Oak Ridge National Laboarotry, Katsaras, John; Oak Ridge National Laboratory, Neutron Sciences Directorate Sumpter, Bobby; Oak Ridge National Laboratory, Computer Science and Mathematics Division and Center for Nanophase Materials Sci Ashkar, Rana; Virginia Polytechnic Institute and State University, Physics Kumar, Rajeev; Oak Ridge National Laboratory, Center for Nanophase Materials Sciences

SCHOLARONE™
Manuscripts

Cite this: DOI: 00.0000/xxxxxxxxxx

The Influence of Curvature on Domain Distribution in Binary Mixture Membranes[†]

Wei Li,^{a‡} Jan-Michael Y. Carrillo,^{*ab} John Katsaras,^{cde} Bobby G. Sumpter,^{ab} Rana Ashkar^{*fg} and Rajeev Kumar^{*ab}

Received Date

Accepted Date

DOI: 00.0000/xxxxxxxxxx

Curvature-induced domain sorting, a strategy exploited by cells to organize membrane components, is a promising mechanism to control self-assembly of materials. To understand this phenomenon, this work explores the effects of curvature on component rearrangement in thin polymer films and lipid bilayers supported on sinusoidal substrates. Specifically, self-consistent field theory (SCFT) was used to study the spatial distribution of polymers in blends containing conformationally asymmetric chains. In tandem, coarse-grained molecular dynamics (MD) simulations were used to probe the arrangement of rigid lipid domains in a relatively soft lipid matrix. Besides the expected preference of rigid species localizing in regions with low mean curvature, both systems exhibit unexpected localization of rigid components in comparatively high curvature regions. Origins of this unexpected sorting are discussed in terms of entropic and enthalpic contributions. This study demonstrates that domain distribution strongly depends on local topography and further highlights the collective effects that thermodynamic forces have on the morphological behavior of membranes.

1 Introduction

Understanding self-assembly under geometric frustration in soft matter systems is central to the development of next generation materials.¹ A grand challenge in designing such materials relates to the fact that spatial frustration tends to favor assemblies with local packing motifs that are not necessarily predicted by bulk thermodynamics. A prime example of this, is the stabilization of defects or heterogeneities by curvature.^{1,2} In biology, there is ample evidence that cells use curvature to regulate structure and function.³ For instance, *Bacillus subtilis*, a rod-shaped bacterium

known to endure extreme environmental conditions, uses curvature to ensure its survival.⁴ During sporulation, the bacterial membrane localizes cardiolipin clusters to its curved poles, which enables the recruitment of vital proteins.^{5,6} Other examples of cellular membranes that exploit curvature to induce structural rearrangement and control cellular functions include the golgi apparatus, endoplasmic reticulum, and mitotic cleavage furrows.^{7,8}

Despite the recognition of curvature as an important structural feature for controlling the spatial organization of biomolecules in the plasma membrane (e.g., lipids and proteins), the mechanism responsible for curvature-mediated membrane rearrangement is still not fully understood.^{3,8,9} To take advantage of membrane curvature strategies used in nature, it is necessary to discern the complex coupling between membrane topography and emergent in-plane structures in a general class of geometrically frustrated self assemblies. Studies in this direction will eventually establish new design rules for soft materials that will, in most likelihood, be different than those utilized currently.⁸ Here, we focus on two commonly studied soft matter systems, namely, polymer films and lipid bilayers.

For lipid membranes, numerous studies have focused on various degrees of curvatures, ranging from the nanoscale curvature of lipid nanotubes pulled out of giant unilamellar vesicles^{10,11}, to mesoscopic curvatures of membranes supported on lithographically patterned substrates⁹, and even micron-scale curvatures of membranes on wrinkled or buckled polymer substrates¹². Ex-

^a Center for Nanophase Materials Sciences, Oak Ridge National Laboratory, Oak Ridge, Tennessee 37831, United States; E-mail: carrillojy@ornl.gov; Email: kumarr@ornl.gov

^b Computational Sciences and Engineering Division, Oak Ridge National Laboratory, Oak Ridge, Tennessee 37831, United States

^c Neutron Scattering Division, Oak Ridge National Laboratory, Oak Ridge, Tennessee 37831, United States

^d Department of Physics and Astronomy, University of Tennessee, Knoxville, Tennessee 37996, United States

^e Shull Wollan Center: a Joint Institute for Neutron Science, Oak Ridge National Laboratory, Oak Ridge, Tennessee 37831, United States

^f Department of Physics, Virginia Polytechnic Institute and State University, Blacksburg, Virginia 24061, United States; Email: ashkar@vt.edu

^g Center for Soft Matter and Biological Physics, Virginia Tech, Blacksburg, Virginia 24061, United States

[†] Electronic Supplementary Information (ESI) available: See DOI: 10.1039/cXsm00000x/

[‡] Present address: Center for Computation & Theory for Soft Materials, Northwestern University, Evanston, Illinois 60208

perimental^{9,12,13} and theoretical^{14–17} results have shown that curvature can induce lipid phase-separation and that the resultant phase-sorting depends on membrane topography. Theoretical studies have also revealed that large differences in bending rigidities of lipid domains are needed to stabilize certain domain patterns.¹⁵ These studies^{9,13,15} have shown that in a membrane containing two types of coexisting lipid domains, domains with higher bending rigidity get localized in spatial regions with low mean curvatures in order to avoid a bending energy penalty.

In comparison, research on curvature-induced sorting in polymer blends is limited, but few studies on homopolymer adsorption on rough surfaces have pointed to important effects in the interplay between substrate curvature and polymer conformational properties in determining localization in regions with varying curvatures.^{18–23} In spite of these findings, commonalities and differences in curvature-induced domain localization are yet to be understood.

In this work, we present results related to curvature-induced domain localization on an experimentally realizable surface for the two aforementioned soft matter systems. Two analogous models were constructed for ultra-thin films or membranes containing binary mixtures of polymers and lipids, respectively. In these models, effects resulting from asymmetry between the top and bottom layers of the membranes were neglected, while the mean curvature was controlled by varying the substrate topography. In particular, sinusoidal substrates were considered to emphasize the effects of mean curvature and avoid any effects from Gaussian curvature. It can also be readily shown that the analog of bending rigidity differences between lipid domains is the contrast in the Kuhn segment lengths of the polymers (see the Electronic Supplementary Information, ESI†, for details), which can be varied to control sorting of phase-separated polymeric domains. We will examine morphological changes due to variations of the surface curvature and underlying thermodynamic driving forces are discussed.

2 Results & Discussions

2.1 Polymer Blend Thin Films

Polymeric films containing a blend of monodisperse A and B homopolymers were simulated using self-consistent field theory (SCFT). A model was constructed for a corrugated thin film in the canonical ensemble^{24,25} with A and B polymers represented by continuous Gaussian chains. Two types of polymers were used having the same degree of polymerization N , but different Kuhn segment lengths (l_K). In particular, the Kuhn length of A-segments, l_A , was kept fixed while the ratio $\eta_K = l_B/l_A$ (referred to as the conformational-asymmetry parameter) was varied. It should be noted that, in general, a larger Kuhn segment length implies a larger persistence length and associated with relatively rigid polymers.²⁶ The Flory–Huggins interaction parameter, χ , describing short-ranged pairwise interactions between A and B segments, was chosen so that $\chi N > 2$ led to phase-separated polymeric domains²⁴. Furthermore, the volume fractions of A and B polymers in the film at a location \mathbf{r} were denoted as $\phi_A(\mathbf{r})$ and $\phi_B(\mathbf{r})$, respec-

tively. The confining substrates were implemented by the masking method^{25,27} with fixed density profiles expressed as $\phi_w(\mathbf{r}) = 1 + [\tanh\{(z - u_1(x))/\zeta_1\} - \tanh\{(z - u_0(x))/\zeta_0\}]/2$, where u_0 and u_1 represent sinusoidal surfaces centered at $z = z_0$ and $z = z_1$, respectively. ζ_0 and ζ_1 represent the widths of the substrate-polymer interfaces located at $z = z_0$ and $z = z_1$, respectively. Specifically, both surfaces were assumed to have the same widths (i.e., $\zeta_0 = \zeta_1 \ll R_{gA}$) and sinusoidal corrugations along the x direction such that $u_0(x) - z_0 = u_1(x) - z_1 = a \sin(2\pi x/\lambda)$ and $|z_1 - z_0| = h$ characterized the film thickness. Preliminary SCFT results indicate that lateral phase segregation is more pronounced for more confined systems (results not shown). The film thickness was chosen to be $0.8(N/6)^{1/2}l_A$ in order to concentrate on strongly confined films and to compare with lipid bilayer results. The SCFT calculations were performed in real space using a pseudo-spectral algorithm with periodic boundary conditions using PolySwift⁺⁺.^{24,28,29} To highlight any entropic effects resulting from conformational asymmetry, we omitted interactions between the substrates and the polymers.

Conformational asymmetry affects surface segregation behavior of polymers in blends. In particular, polymers with smaller Kuhn segment lengths prefer to accumulate close to the surface, as they experience less entropy loss when at the interface^{30–32} (see the ESI†). In addition, conformational asymmetry can affect lateral phase segregation of polymers on corrugated surfaces. As shown in Fig. S1 for the case of $\phi_B = 0.2$, the B-rich phase is transposed from the peak (or valley) to the flat region as η_K increases. This *entropy-driven* (see Fig. S1 in ESI†) morphological transition implies that positioning less flexible polymers in the high curvature region increases entropy losses and hence, the free energy. This clearly shows that the topographic feature and Kuhn segment length are coupled in the free energy and our theoretical analysis for a polymer melt near a sinusoidal surface corroborates this conclusion (see the ESI†). From SCFT calculations at different ϕ_B (cf. different panels in Fig. S3 of the ESI† for the B density profiles in systems of $a = 1.4$ at various λ), we infer that curvature has a much larger effect in determining domain localization than the composition of the polymer blend.

Curvature-induced sorting in polymer blends can be rationalized by considering entropic effects near surfaces. Entropic considerations (see ESI† for details) reveal that the curvature effects for polymer melts near a sinusoidal surface are significant in the limits of $\lambda < 1.81R_{gj}$ and $a > 0.47R_{gj}$, where $R_{gj} = (N/6)^{1/2}l_j$, $j = A, B$. In these limits (see Eq. S7 in ESI†), the local entropic cost (in units of thermal energy and per unit area) for occupying a curved region contains contributions such as $\sim \rho_0(Nl_j^4/\zeta_0)(\partial^2 u_0/\partial x^2)^2 \sim \rho_0 N l_j^4 a^2/\zeta_0 \lambda^4$ and $\sim \rho_0(Nl_j^4/\zeta_0^3)(\partial u_0/\partial x)^4 \sim \rho_0(Nl_j^4/\zeta_0^3)(a/\lambda)^4$, where ρ_0 is number density of polymer chains. This implies that the loss of entropy for occupying highly curved regions near peaks and valleys is less if polymers with smaller Kuhn segment lengths get localized there. In the limit of weak-curvature (see Eq. S7 in ESI†) such that $a/\lambda \rightarrow 0$, the local entropic cost scales as $\sim (l_j^2/\zeta_0)(\partial u_0/\partial x)^2$, which implies that polymers with smaller Kuhn segment length preferentially localize in regions near peaks and valleys, where lateral spatial gradients are maximum. In other words, polymers with smaller Kuhn segment lengths are

entropically favored in curved regions near peaks and valleys for all values of a and λ .

To probe additional curvature effects, we systematically varied film corrugation by changing a and λ . In Fig. 1(a) we show monomer volume fraction profiles of B with a mixing ratio of B:A of 1 : 9, and $\eta_K = 2.0$ for different values of a and λ . For comparison, the planar thin film ($a = 0$, data not shown) is in the one-phase region, *i.e.*, the polymer density distribution is laterally homogeneous, while the B density profile exhibits a symmetric bimodal distribution along the film thickness direction (with two relatively high density layers close to the walls). The system shows similar behavior at small a and large λ , as in the case of $a = 0.6$ and $\lambda = 10.24$ in Fig. 1(a). With decreasing λ and increasing a , curvature increases and its effects become more pronounced, promoting phase separation between A and B. Moreover, two types of B-rich phase domain distributions are observed: the B-rich phase remains in the low curvature slope region at small λ , but shifts to the high curvature region with increasing λ . In order to clarify the effects of the local mean curvature in the sorting of phase-separated polymer domains, we plotted the local curvature for the sinusoidal surface with $a = 1.4$ in Fig. 1(b). These figures clearly show that coupling between local mean curvature and conformational asymmetry can lead to domain sorting in phase segregating polymer blends.

Thermodynamic stability of the counter-intuitive morphologies at large λ was studied by using the SCFT calculations from different initial configurations. As shown in Fig. 1(c) for the system at $a = 1.4$, B-rich phases were initially located in the slope region, but relocated to the high curvature region after the SCFT calculation converged. Fig. 1(d) shows that the final states have lower free energies and are thermodynamically stable. In particular, the entropic part provides the main driving force for transition in morphologies, compared to the change in the enthalpic part ($U \sim \int \chi N \phi_A(\mathbf{r}) \phi_B(\mathbf{r}) d\mathbf{r}$). Consideration of interactions with substrates in the weak-curvature limit (*i.e.*, $a/\lambda \rightarrow 0$) reveals that repulsive monomer-surface interactions lead to polymers localizing in the highly curved regions. Specifically, less flexible polymers are entropically repelled from the surface and are localized in high-curvature regions due to a decrease in the local surface area of the differential element on a sinusoidal surface in contrast to its reference planar surface (see Fig. S2 in ESI†). Similarly, attractive monomer-surface interactions lead to localization of the polymers in low-curvature regions due to the increase in local surface area in those regions. Overall, we find that less flexible polymers preferentially segregate in low-curvature or slope regions in the limit where surface curvature is significant, but can localize in highly curved regions due to a higher entropic repulsion from the surface.

To visualize the coupling between local curvature and domain localization in the polymer blends, we focused on a layer close to one of the substrates. Specifically, we analyzed the volume fractions of B at the peak (*i.e.*, at $x = \lambda/4$) and at the middle (*i.e.*, at $x = \lambda/2$) of the sinusoidal corrugation, denoted as ϕ_B^p and ϕ_B^m , respectively. The distributions of ϕ_B^p and ϕ_B^m as a function of a and λ are summarized in Fig. 2(a) and (b), respectively, which delineate the surface segregation behavior of the B poly-

mers in the high and low curvature regions. The ratio of ϕ_B^m/ϕ_B^p in Fig. 2(c) can be considered as an order parameter that describes the spatial distribution of domains based on local curvature. Thus, Fig. 2(c) serves as a schematic phase diagram for domain sorting. For reference, the colormap of the average substrate absolute mean curvature $\langle |H| \rangle = \int_0^\lambda |u''(x)| [1 + u'(x)^2]^{-3/2} dx / 2\lambda = 4\pi a (\lambda^4 + 4\pi^2 a^2 \lambda^2)^{-1/2}$ ^{33,34} is shown in Fig. 2(d).

Fig. 2(c) shows preferential tendency of the B polymers to reside in the low curvature region ($\phi_B^m/\phi_B^p > 1$, denoted as Type-I sorting) when λ is small; this behavior becomes more pronounced at large a , in accord with an increase in the average substrate mean curvature (Fig. 2(d)). By contrast, the other type of domain sorting ($\phi_B^m/\phi_B^p < 1$, denoted as Type-II sorting) emerges only at large λ and includes smaller values of λ with increasing a . In general, the schematic phase diagram captures the properties of entropic domain sorting, which we attribute to the interplay between the polymer Kuhn segment lengths and the surface topography. We expect that this entropy-driven domain sorting generally exists in binary phase-separating systems when two components experience different entropy losses as a result of geometric frustration.

2.2 Binary Lipid Membranes

The behavior of curvature-induced domain sorting in lipid bilayers under similar geometric modulation was studied using molecular dynamics (MD) simulations. A detailed description of the coarse-grained model and simulation procedure can be found in the ESI†. Briefly, we constructed a phase-separating system containing N_A number of A lipids and N_B number of B lipids, with B being the minority component. We adopted the Cooke–Deserno model^{35,36} where each lipid is represented by three beads (see Fig. S4 in ESI†) and connected via anharmonic springs. The lipid stiffness was controlled by an angle potential.³⁷ The bead representing the lipid headgroup (of size 0.95σ) was purely repulsive to other lipid beads, and the tail beads (of size σ) interacted with each other through a hard-core repulsion and a long-range attraction, which qualitatively resulted in the required hydrophobic balance. A pure A-lipid domain had an estimated bending rigidity of $\kappa_A = 10.4 k_B T$ ($k_B T$ is thermal energy), while a pure B-lipid domain was stiffer with $\kappa_B = 52.3 k_B T$.³⁷ The line tension between A and B domains was estimated to be $\Sigma_{AB} = 3.56 k_B T / \sigma$ (see ESI†). The supporting substrate had a topography described by the sinusoidal function $u(x) = a \sin(2\pi x / \lambda)$ along the x axis and had *attractive* interactions with the head beads, and an interaction strength that is independent of lipid type. Periodic boundary conditions were enforced in the lateral x and y directions. Simulations were performed in the canonical ensemble with a Langevin thermostat using the LAMMPS MD simulation package.^{38,39} Standard Lennard–Jones (LJ) reduced units were used in the simulations and length scales were in units of σ .

MD simulations were started with a random bilayer membrane deposited onto the substrate. Demixing of the A and B lipids took place as the simulation proceeded, resulting in the formation and growth of B-lipid domains. The coarsening of the B domains served to reduce any unfavorable contact between A and B lipids.

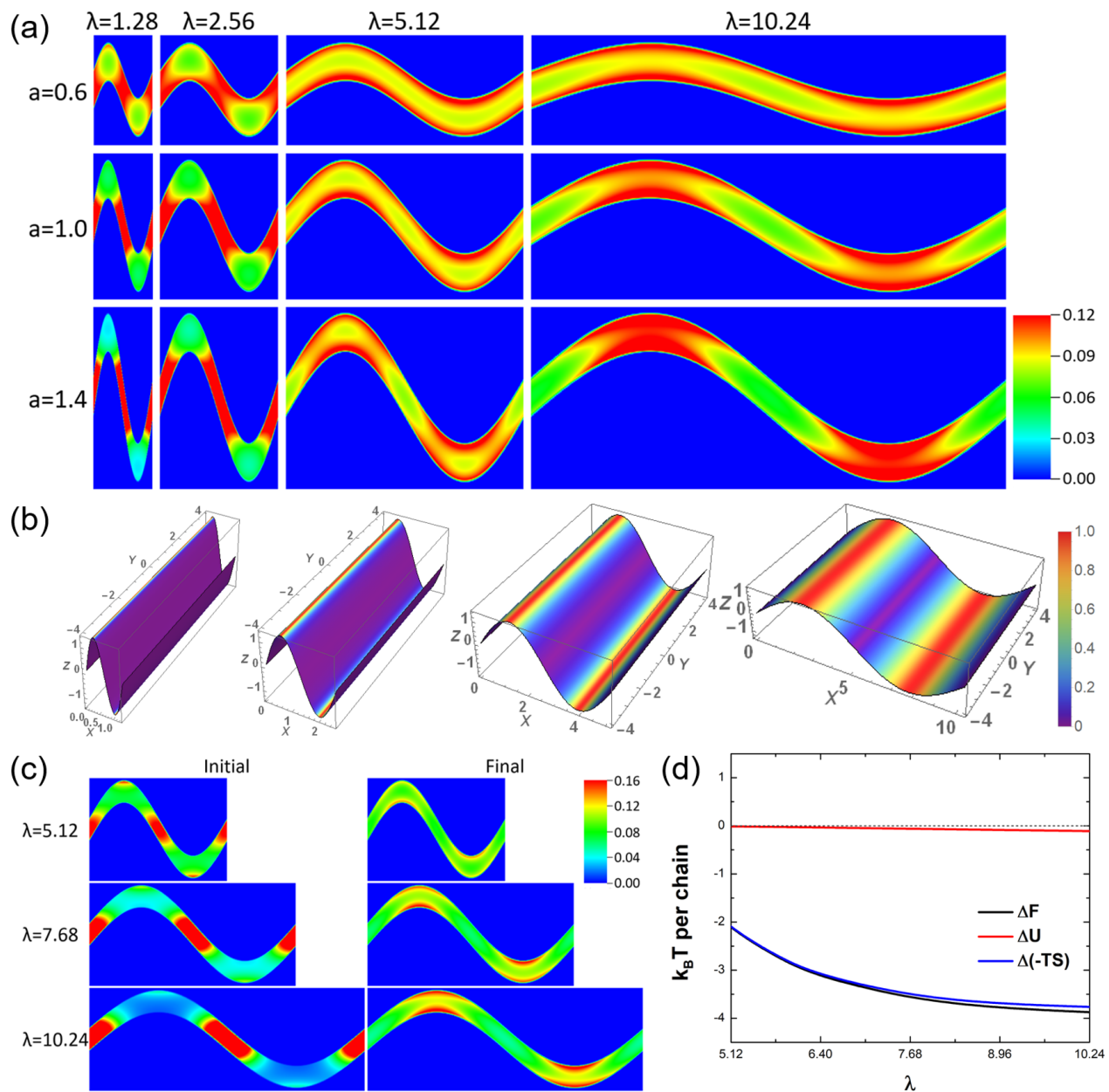


Fig. 1 (a) SCFT based monomer volume fraction profiles of the B polymers in a blend (mixing ratio of B to A of 1 : 9) confined between sinusoidally corrugated thin films with $h = 0.8$, $\chi = 0.1$, $N = 60$, and $\eta_K = 2$ at different corrugation wavelengths, λ , and amplitudes, a . (b) Colormaps of the normalized mean curvature ($|H| = \frac{1}{2}|u''(x)|[1 + u'(x)^2]^{-3/2}$) with respect to their maximum values on sinusoidally corrugated surfaces of $a = 1.4$ with $\lambda = 1.28$, 2.56, 5.12, and 10.24. (c) SCFT based monomer volume fraction profiles of B in initial and converged final states for different λ systems and $a = 1.4$. (For visualization purposes, the color bar was changed from the one used in panel (a)). (d) Differences in the total free energy (ΔF), enthalpic (ΔU), and entropic changes ($\Delta(-TS)$, T is temperature) between the final and the initial states as a function of λ . Length scales are in units of $R_{gA} = (N/6)^{1/2}l_A$, where R_{gA} is the unperturbed radius of gyration of the A polymer.

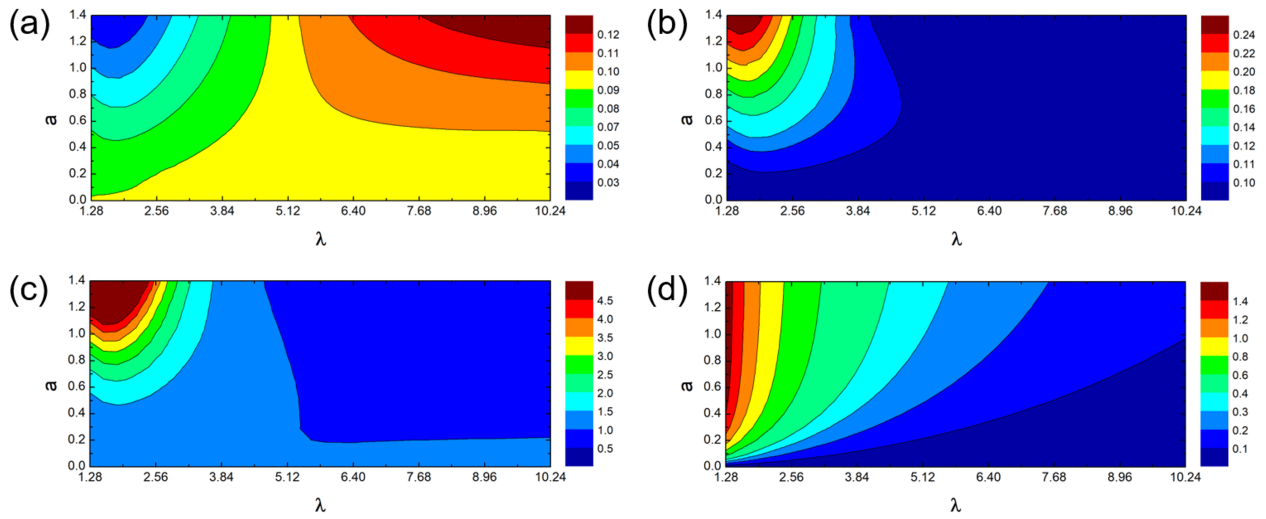


Fig. 2 Distribution of the B polymer as a function of corrugation amplitude, α , and wavelength, λ , in thin films with $h = 0.8$, $\phi_B = 0.1$, $\chi N = 6$, and $\eta_K = 2$ for: (a) monomer volume fraction of B (ϕ_B^p) near the substrate and at the peak of the sine wave ($x = \lambda/4$); (b) monomer volume fraction of B (ϕ_B^m) near the substrate and at the middle of the slope ($x = \lambda/2$); (c) ratio of ϕ_B^m/ϕ_B^p ; and (d) average substrate mean curvature $\langle |H| \rangle$. The length scales are in units of R_{gA} and curvature in units of R_{gA}^{-1} .

In addition to coarsening, individual B domains merged with each other to form larger aggregates. This process relies on cluster diffusion and was significantly retarded as B domains grew in size and became farther apart. Later on, the system reached a steady state with scattered B domains residing in a continuous phase of A lipids. We note that the steady state may not be the thermodynamic equilibrium, and the size and location of lipid domains depend on the initial simulation configuration. To extract statistical information about the thermodynamic force on domain localization, we performed simulations for eight different concentrations of $\rho_B = 0.05, 0.10, 0.15, 0.20, 0.25, 0.30, 0.35, 0.40$ and for four different substrate wavelengths (see Tab. S1 in ESI[†] for the system sizes). For each combination, we ran three independent simulations using different initial lipid positions and velocities. In Fig. 3, we show typical snapshots of the steady states in planar and modulated membranes (see Figs. S6 and S7 in ESI[†] for the kinetic details of the phase separation process).

For assessing the equilibrium states, we survey the analysis presented in Ref.¹⁵ In particular, Fig. 3 in Ref.¹⁵ shows that the equilibrium distribution of lipid domains on a corrugated substrate can be estimated by comparisons between an elastic length scale, ξ_{el} , and a topographical length scale, ξ_{to} , in addition to the concentration of domains. We estimated the elastic length scale, $\xi_{el} = (\kappa_B - \kappa_A)/\Sigma_{AB} = 11.75\sigma$. However, it is not straightforward to compute ξ_{to} from the MD simulations of sinusoidal surfaces due to difficulties in mapping the sinusoidal surface to a representation based on cylindrical arcs and inclined planes, as done in Ref.¹⁵. Given these limitations and the fact that the simulations might not reach the equilibrium state, we cannot confirm that the equilibrium distribution of domains can either be two macrophase separated domains spanning multiple curved regions or broken stripe domains exhibiting rigid domains in low curvature regions. However, it is important to note that the effects of entropy due to the finite range of the interfacial interactions and the exclusion

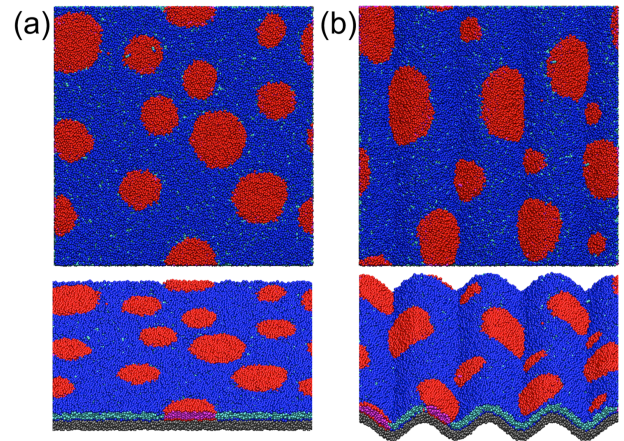


Fig. 3 Typical snapshots of the simulation cell with (a) planar ($\alpha = 0$) and (b) corrugated substrates ($\alpha = 5$, $\lambda = 10\pi$), showing domains of minority (red) B lipids (with a number fraction of $\rho_B = N_B/(N_A + N_B) = 0.15$). The equilibrium area per lipid is $1.23 \sigma^2$ and $1.08 \sigma^2$ for A and B lipids, respectively.

from the interfaces were not considered in Ref.¹⁵. This said, we expect these entropic effects as considered in the SCFT calculations, to stabilize the localization of rigid domains in high curvature regions, even at equilibrium. These observations can have significant biological implications in transient membrane reorganization during cellular processes. The ability of small raft-like domains to localize at the peripheral highly-curved portions of a membrane could facilitate protein binding and signaling events.

In modulated membranes, the corrugation hinders the coalescence of B-lipid domains. According to Helfrich,⁴⁰ the bending energy per unit area of a lipid membrane is $f_{bend} = \frac{1}{2}\kappa(2H - H_0)^2 + \tilde{\kappa}K$, where κ is the mean curvature modulus (also known as the bending rigidity), and $\tilde{\kappa}$ is the Gaussian curvature modulus; H , H_0 , and K are the mean, spontaneous, and Gaussian

curvatures, respectively. By mapping the coarse-grained lipid bilayer to the continuum model, one finds that $H_0 = 0$ and $K = 0$ for the membranes exhibiting the same distribution of lipids on both leaflets and sinusoidal surfaces, respectively. Hence, $f_{bend} = 2\kappa H^2$. This implies that having rigid B-lipid domains in high curvature regions of a sinusoidal surface, instead of the vicinity of soft A-lipid domains, results in an increase in the total bending energy (*i.e.*, $\sim \int_S 2(\kappa_B - \kappa_A)H(x)^2 dx dy$ over the area S , which is positive as $\kappa_B > \kappa_A$). Therefore, rigid B domains preferentially localize in low curvature regions to reduce the bending energy penalty, resulting in *enthalpy-driven* domain sorting. In other words, the larger the curvature, the stronger the sorting effect. Furthermore, while undergoing sorting, B domains become elongated to accommodate the ridge topographical feature, in contrast to their more rounded shape in the planar case when under line tension. Our findings are in good agreement with the results from previous experimental and theoretical studies.^{9,15}

To explore connections between domain localization and lipid domain size, we performed data analysis on the average domain mean curvature. Specifically, the membrane surface was discretized into a two-dimensional grid with uniform projected separations along the x and y axes (see Fig. S5 in ESI†). The grid length in the x direction was taken to be equal to the arc length on the sine wave over the separation in x . The average mean curvature of a domain was estimated by $|H_d| = \sum_{ij}^d |H_{ij}| \Delta x_i \Delta y_j / A_d$, where i and j are grid indices inside the domain. $H_{ij} = \frac{1}{2} u''(x_i) [1 + u'(x_i)^2]^{-3/2}$ is the mean curvature^{33,34} at $x = x_i$, d is the total number of grid points in a domain, $A_d = \sum_{ij}^d \Delta x_i \Delta y_j$ is the domain area, and Δx_i and Δy_j (which is invariant) are the grid spacings along x and y , respectively. In Fig. 4(a) we plot $|H_d|$ with respect to A_d for systems with $\lambda = 10\pi$, 20π , and 40π . These curves were obtained by binning $|H_d|$ and A_d for all B-lipid domains in the time window of $1 \times 10^4 \tau$ to $8 \times 10^5 \tau$ (at an interval of $5 \times 10^3 \tau$) from simulations of different ρ_B in the x -axis by a bin size of $5\sigma^2$ (see demonstration in Fig. S8 of the ESI†). The average mean curvature of the substrate surface is $\langle |H| \rangle = \sum_{ij} |H_{ij}| \Delta x_i \Delta y_j / \sum_{ij} \Delta x_i \Delta y_j$, which is marked accordingly for the cases we studied. Due to almost complete conformity of the lipid domains with the substrate, $|H_d| < \langle |H| \rangle$ corresponds to the localization of B domains in low curvature regions, and vice versa.

The distribution curves in Fig. 4(a) reveal characteristics of the domain sorting effect. For example, at large λ and A_d , the domain mean curvature, $|H_d|$, fluctuates around the surface mean curvature, $\langle |H| \rangle$, implying that domain sorting is relatively weak for low curvatures and large domains. As λ decreases and $\langle |H| \rangle$ increases, the sorting effect becomes more pronounced. At $\lambda = 10\pi$ and 20π , $|H_d|$ goes below $\langle |H| \rangle$ as A_d reduces, suggesting that intermediate-sized rigid domains are mostly situated in low curvature regions (*i.e.*, Type-I sorting). Nevertheless, as A_d further decreases, $|H_d|$ shows a marked upturn, exceeding $\langle |H| \rangle$. This points to the other type of domain sorting that we observed in the polymer thin films, namely that rigid B domains are accommodated in high curvature regions (*i.e.*, Type-II sorting). We note that this sorting behavior persists regardless of simulation time (see snapshot shown in Fig. S9 of ESI† for small B-lipid domains in the peak area at the end

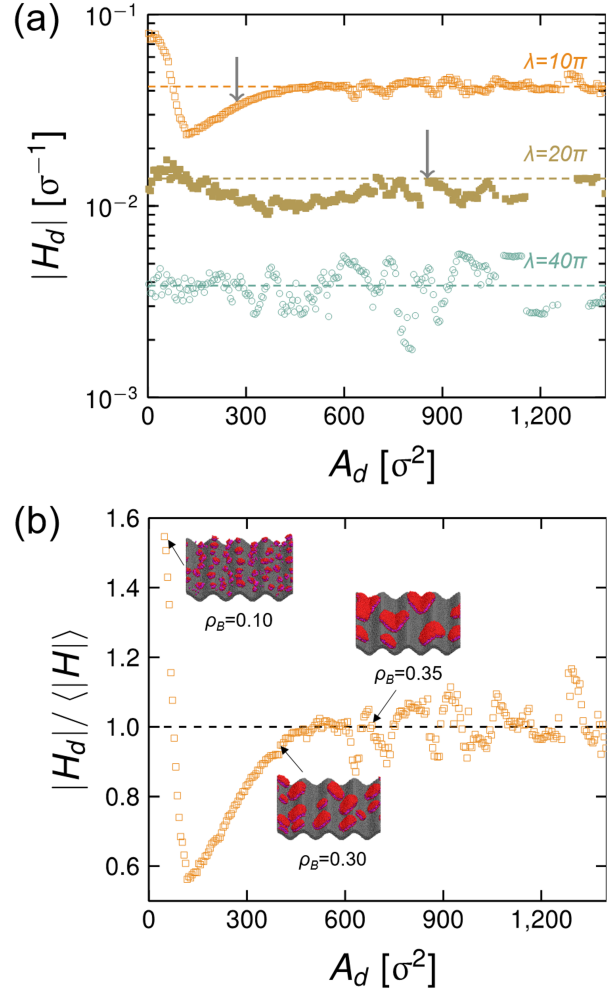


Fig. 4 (a) Distribution of average domain mean curvature, $|H_d|$, as a function of domain area, A_d , for systems with different λ and $a = 5$. Changes to A_d were obtained from simulations of different B lipid densities. The average surface mean curvatures are 0.042, 0.0139, and 0.0038 (in units of σ^{-1}) and are indicated by the horizontal dashed lines. Arrows indicate the cases of $A_d = \pi r_c^2$, where $r_c = \sqrt{(2a)^2 + (\lambda/2)^2} / 2$. The values correspond to the area of maximum circles that can approximately fit in the slope area between the peak and valley. (b) Distribution of the normalized average domain mean curvature, $|H_d| / \langle |H| \rangle$, for the system $\lambda = 10\pi$. Typical snapshots of B-lipid domains formed on the substrate at different ρ_B and simulation timesteps are shown as insets.

of the simulation). To elucidate the morphological differences between the two types of domain sorting, we plot the distribution of normalized domain mean curvature, $|H_d|/\langle |H| \rangle$, for the system with $\lambda = 10\pi$ and show typical snapshots of B-lipid domains in Fig. 4(b), where $|H_d|/\langle |H| \rangle = 1$ separates the two sorting behaviors.

From the findings in the thin films of binary polymer blends, we infer that the localization of small rigid B-lipid domains in the high curvature region has thermodynamic origins and is driven by the same entropic considerations. The MD results suggest that this entropic effect could persist under thermal fluctuations when the surface mean curvature is sufficiently large. Accordingly, one would expect that the domain sorting behavior in lipid membranes may exhibit a behavior similar to what is shown in Fig. 2(c). Therefore, by reducing λ at a fixed corrugation amplitude, a , the system first undergoes Type-II sorting when the sorting effect becomes significant. Moreover, the stability region of Type-II sorting can be greater than Type-I sorting (the boundary between the two may shift slowly by varying the volume fraction of B). We note that the binary lipid system indeed displays Type-II sorting first (when $|H_d| > \langle |H| \rangle$) as λ decreases, and when A_d is small. However, unlike the polymer model that only involves repulsive interactions, lipid tail beads interact with each other through an attractive potential. These attractive potentials collectively introduce an energy penalty related to the bending of the lipid domains. This energy penalty depends on the bending rigidity, curvature, and domain size. Type-I sorting is also enthalpically more favorable as it has a lower bending energy, compared to Type-II sorting. Such an enthalpic driving force increases with increasing the domain size, facilitating the transition in domain sorting and spatial localization (Fig. 4(b)). Hence, Type-II sorting only exists in the case of small B-lipid domains, either in small ρ_B systems or at the early demixing stage of large ρ_B systems, where entropic effects dominate.

3 Conclusions

In summary, we have studied the effect of curvature on the distribution of binary components in two types of thin films. Under a sufficiently large surface mean curvature, the spatial rearrangement of film components is associated with substrate topography. A general finding is that rigid species are not always accommodated in low curvature regions (Type-I sorting), but in some circumstances, can be located in high curvature regions (Type-II sorting). For the confined polymer blend, SCFT calculations showed that two polymer species with different Kuhn lengths compete for the curved regions to minimize loss of entropy. This competition results in two types of domain sorting associated with the size of the topographic feature and the polymer blend components. Similar domain sorting behaviors were shown to exist in lipid bilayer membranes by MD simulations. In addition to the entropic driving force in the polymer system, the intermolecular association between lipid molecules results in the coupling of curvature with bending rigidity and domain size via the bending energy. The resulting enthalpic driving force favors Type-I over Type-II sorting in the lipid system. Accordingly, the presence of B-lipid domains in high curvature regions was observed only

when the domain size is small enough for entropic effects to be significant. Our findings suggest possible mechanisms by which curvature-induced domain sorting in soft matter systems can take place. They also point to how biological membranes can use local curvature to sort molecular assemblies and how such strategies developed by cells can be employed in developing new designs of engineered thin films.

Conflicts of interest

There are no conflicts of interest to declare.

Acknowledgements

This research was performed at the Center for Nanophase Materials Sciences, which is a US Department of Energy Office of Science User Facility. This research used resources of the Oak Ridge Leadership Computing Facility at the Oak Ridge National Laboratory, which is supported by the Office of Science of the U.S. Department of Energy under Contract No. DE-AC05-00OR22725. J.K. is supported through the Scientific User Facilities Division of the Department of Energy (DOE) Office of Science, sponsored by the Basic Energy Sciences (BES) Program, under Contract No. DE-AC05-00OR22725.

References

- 1 G. M. Grason, *J. Chem. Phys.*, 2016, **145**, 110901.
- 2 D. Nelson, T. Piran and S. Weinberg, *Statistical Mechanics of Membranes and Surfaces*, World Scientific Pub., 2004.
- 3 P. Bassereau, R. Jin, T. Baumgart, M. Deserno, R. Dimova, V. A. Frolov, P. V. Bashkurov, H. Grubmüller, R. Jahn, H. J. Risselada, L. Johannes, M. M. Kozlov, R. Lipowsky, T. J. Pucadyil, W. F. Zeno, J. C. Stachowiak, D. Stamou, A. Breuer, L. Lauritsen, C. Simon, C. Sykes, G. A. Voth and T. R. Weikl, *J. Phys. D: Appl. Phys.*, 2018, **51**, 343001.
- 4 M. T. Madigan, J. M. Martinko and J. Parker, *Brock Biology of Microorganisms*, Prentice Hall Upper Saddle River, NJ, 1997, vol. 11.
- 5 K. C. Huang, R. Mukhopadhyay and N. S. Wingreen, *PLOS Comput. Biol.*, 2006, **2**, e151.
- 6 K. J. Boyd, N. N. Alder and E. R. May, *Langmuir*, 2017, **33**, 6937–6946.
- 7 M. Okamoto, K. Kurokawa, K. Matsuura-Tokita, C. Saito, R. Hirata and A. Nakano, *J Cell Sci*, 2012, **125**, 3412–3420.
- 8 R. Parthasarathy and J. T. Groves, *Soft Matter*, 2006, **3**, 24–33.
- 9 R. Parthasarathy, C.-h. Yu and J. T. Groves, *Langmuir*, 2006, **22**, 5095–5099.
- 10 B. Sorre, A. Callan-Jones, J.-B. Manneville, P. Nassoy, J.-F. Joanny, J. Prost, B. Goud and P. Bassereau, *Proc. Natl. Acad. Sci.*, 2009, **106**, 5622–5626.
- 11 M. Heinrich, A. Tian, C. Esposito and T. Baumgart, *Proc. Natl. Acad. Sci.*, 2010, **107**, 7208–7213.
- 12 S. F. Gilmore, H. Nanduri and A. N. Parikh, *PLOS ONE*, 2011, **6**, 1–8.
- 13 A. Tian and T. Baumgart, *Biophys. J.*, 2009, **96**, 2676–2688.

- 14 M. Mercker, T. Richter and D. Hartmann, *J. Phys. Chem. B*, 2011, **115**, 11739–11745.
- 15 B. Różycki, T. R. Weikl and R. Lipowsky, *Phys. Rev. Lett.*, 2008, **100**, 098103.
- 16 H. Koldsø, D. Shorthouse, J. Hélie and M. S. Sansom, *PLoS Comput. Biol.*, 2014, **10**, e1003911.
- 17 S. Baoukina, H. I. Ingólfsson, S. J. Marrink and D. P. Tieleman, *Adv. Theory Simul.*, 2018, **1**, 1800034.
- 18 D. Hone, H. Ji and P. Pincus, *Macromolecules*, 1987, **20**, 2543–2549.
- 19 A. Baumgaertner and M. Muthukumar, *J. Chem. Phys.*, 1991, **94**, 4062–4070.
- 20 R. Ball, M. Blunt and W. Barford, *J. Phys. A.*, 1989, **22**, 2587.
- 21 W. Sung, J. Sung and S. Lee, *Phys. Rev. E.*, 2005, **71**, 031805.
- 22 Y.-W. Huang and V. K. Gupta, *Macromolecules*, 2001, **34**, 3757–3764.
- 23 A. Venkatakrisnan and V. K. Kuppa, *Curr. Opin. Chem. Eng.*, 2018, **19**, 170–177.
- 24 G. H. Fredrickson, *The Equilibrium Theory of Inhomogeneous Polymers*, Oxford University Press, New York, 2006.
- 25 H. Takahashi, N. Laachi, K. T. Delaney, S.-M. Hur, C. J. Weinheimer, D. Shykind and G. H. Fredrickson, *Macromolecules*, 2012, **45**, 6253–6265.
- 26 M. Rubinstein and R. Colby, *Polymer Physics*, OUP Oxford, 2003.
- 27 M. W. Matsen, *J. Chem. Phys.*, 1997, **106**, 7781–7791.
- 28 S. W. Sides and G. H. Fredrickson, *Polymer*, 2003, **44**, 5859–5866.
- 29 <https://www.txcorp.com>.
- 30 D. T. Wu, G. H. Fredrickson and J. Carton, *The Journal of Chemical Physics*, 1996, **104**, 6387–6397.
- 31 R. Kumar, B. S. Lokitz, S. W. Sides, J. Chen, W. T. Heller, J. F. Ankner, J. F. Browning, S. M. Kilbey II and B. G. Sumpter, *RSC Adv.*, 2015, **5**, 21336–21348.
- 32 A. H. Mah, T. Laws, W. Li, H. Mei, C. C. Brown, A. Ievlev, R. Kumar, R. Verduzco and G. E. Stein, *Macromolecules*, 2019, **52**, 1526–1535.
- 33 S. Safran, *Statistical Thermodynamics Of Surfaces, Interfaces, And Membranes*, CRC Press, 2018.
- 34 F. L. Brown, *Annu. Rev. Phys. Chem.*, 2008, **59**, 685–712.
- 35 I. R. Cooke and M. Deserno, *J. Chem. Phys.*, 2005, **123**, 224710.
- 36 I. R. Cooke, K. Kremer and M. Deserno, *Phys. Rev. E*, 2005, **72**, 011506.
- 37 J.-M. Y. Carrillo, J. Katsaras, B. G. Sumpter and R. Ashkar, *J. Chem. Theory Comput.*, 2017, **13**, 916–925.
- 38 W. M. Brown, P. Wang, S. J. Plimpton and A. N. Tharrington, *Comp. Phys. Comm.*, 2011, **182**, 898–911.
- 39 S. Plimpton, *J. Comp. Phys.*, 1995, **117**, 1–19.
- 40 W. Helfrich, *Z Naturforsch C Bio Sci*, 1973, **28**, 693–703.